NASA TECHNICAL NOTE

NASA TN D-3671

SOME FACTORS INFLUENCING HEAT TRANSFER TO LIQUID-PROPELLANT ROCKET-THRUST-CHAMBER COOLANT CHANNELS

by Roger C. Krueger and Arthur N. Curren

Lewis Research Center
Cleveland, Ohio

NATIONAL AERONAUTICS AND SPACE ADMINISTRATION • WASHINGTON, D. C. • NOVEMBER 1966

NASA TN D-3671

SOME FACTORS INFLUENCING HEAT TRANSFER TO LIQUID-PROPELLANT ROCKET-THRUST-CHAMBER COOLANT CHANNELS

By Roger C. Krueger and Arthur N. Curren

Lewis Research Center
Cleveland, Ohio

NATIONAL AERONAUTICS AND SPACE ADMINISTRATION

For sale by the Clearinghouse for Federal Scientific and Technical Information
Springfield, Virginia 22151 – Price $2.00

SOME FACTORS INFLUENCING HEAT TRANSFER TO LIQUID-PROPELLANT ROCKET-THRUST-CHAMBER COOLANT CHANNELS

by Roger C. Krueger and Arthur N. Curren

Lewis Research Center

SUMMARY

A digital computer program, using finite-difference techniques, was employed to obtain steady-state wall-temperature and heat-flux patterns in the cross section of a rocket-thrust-chamber coolant channel. Several peripheral distributions of the coolant and gas-side heat-transfer coefficients were assumed, and their effects on the wall-temperature and heat-flux patterns compared. The effects of changing the thickness and thermal conductivity of the channel walls and of changing the braze fillet volume of the cross section were also investigated. The channel geometry, fluid temperatures, and heat-flux level were representative of those encountered in an experimental rocket-heat-transfer program conducted at the Lewis Research Center. Experimentally obtained wall temperatures from that program were utilized in assessing the calculated results of this study and in determining which of the assumed heat-transfer-coefficient distributions were most likely to occur.

INTRODUCTION

Among the problems a rocket-thrust-chamber designer must solve is that of providing sufficient cooling to assure adequate product life. Many factors arise to complicate this task; examples include uncertainty of combustion efficiency and possible errors in thermodynamic and transport properties of the propellant or coolant. Another very important factor is the converging-diverging geometry of the chamber, which causes axial changes in the velocity, static temperature, and in many cases the chemical composition of the propellant. Under these conditions, empirical heat-transfer correlations developed for constant-area pipe flow are not adequate. For example, reference 1 presents the axial variations of heat flux for an uncooled thrust chamber and shows that the experimental heat flux at the throat is approximately 40 percent less than a pipe-flow correlation would predict.

Further complications, in the case of regeneratively cooled chambers, result from the fact that the coolant channels form the inner wall of the thrust chamber. Thus, in most designs, the combustion-gas-flow cross section is not circular. Therefore, although the heat flux to the inner wall may be circumferentially uniform in a gross sense (if propellant distribution by the injector is homogeneous), some variation of the gas-side heat-transfer coefficient across each coolant channel may be expected. In such a circumstance, the designer, by assuming a circumferentially constant gas-side heat-transfer coefficient, might successfully predict the heat transfer to the coolant but still incorrectly estimate the maximum wall temperature attained.

Finally, the coolant channels themselves are often not circular tubes, and the principal or only heat flux into them occurs over a fraction of their circumferences. This situation has been only partly investigated. For instance, reference 2 contains analyses of the peripheral heat-flux variation around the inner surfaces of noncircular channels. Reference 3 describes experiments performed with a triangular channel. However, both investigations involve a single channel with heat generation in each wall. Their application to a case of convection heat transfer to part of the periphery may be somewhat remote.

The present investigation was performed to determine whether peripheral variations of the coolant-side heat-transfer coefficient would appreciably affect coolant-channel wall-temperature and heat-flux patterns; to determine if peripheral variations of the gas-side heat-transfer coefficients might exist, and if so the magnitude of those variations; and to explore the effects on wall temperature of changing the thickness and thermal conductivity of the channel walls. To accomplish this, a digital computer program, using finite-difference techniques, was employed. Channel geometry, channel wall properties, and boundary conditions were assumed, and wall-temperature and heat-flux patterns were calculated.

The channel geometry, fluid temperatures, and functions for average values of the heat-transfer coefficients were taken from an experimental rocket-heat-transfer program conducted at the Lewis Research Center. Experimentally obtained wall temperatures from that program were used to assess the calculated results, and to determine which of the assumed gas-side heat-transfer-coefficient distributions was most likely to occur. Finally, the computer program was utilized to determine whether the extra braze material used in the experimental wall thermocouple installations had seriously affected the observed temperature patterns.

The calculations were carried out at an axial location within the region of highest heat flux in the experimental program so that the effects of different assumptions would appear as clearly as possible. The measured wall-temperature patterns and the mode of coolant-channel failure had originally called attention to the fact that appreciable peripheral variations of gas- or coolant-side heat-transfer coefficient, or both, might be occurring.

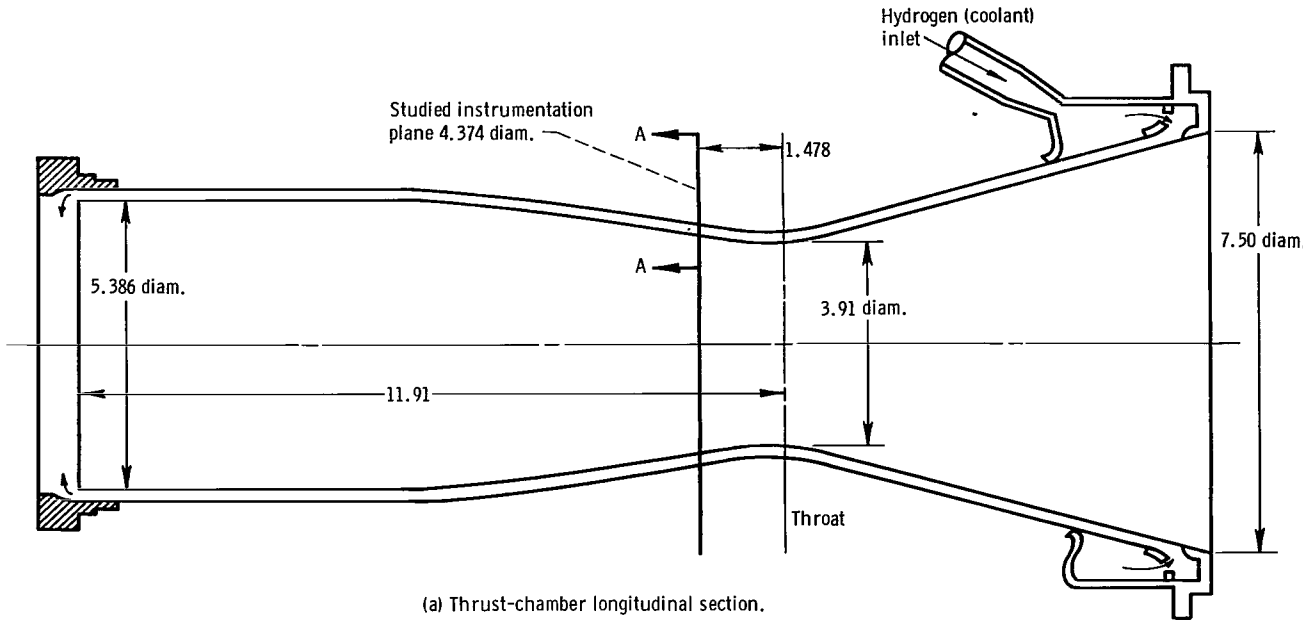

(a) Thrust-chamber longitudinal section.

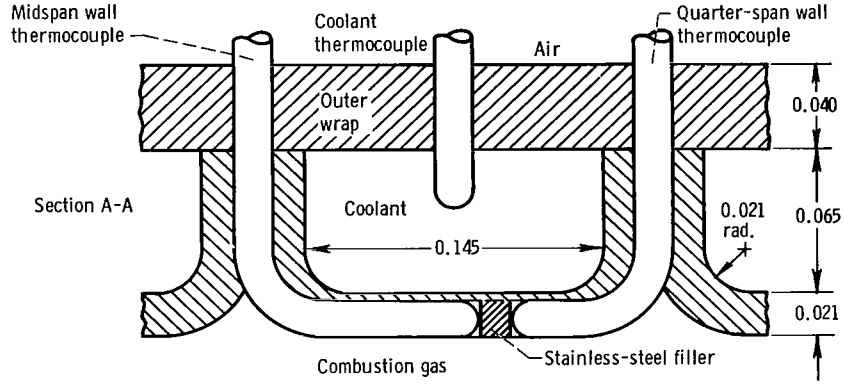

(b) Coolant-channel section at instrumentation plane studied.

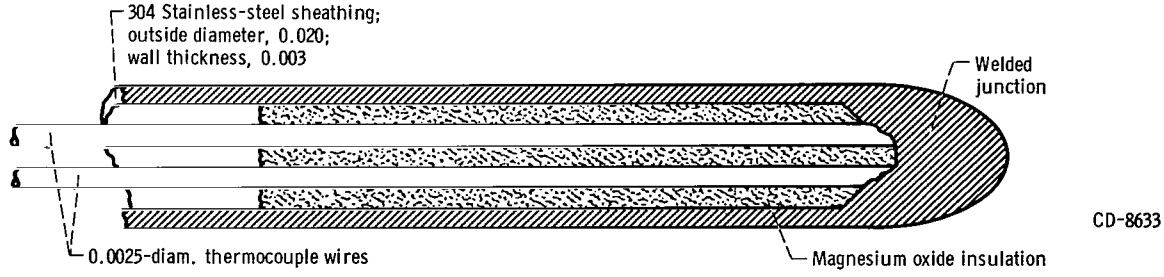

(c) Thermocouple construction. Wall thermocouples, Chromel-Alumel; coolant thermocouples, copper-constantan.

Figure 1. - Experimental chamber, coolant channel, and thermocouple details. (All dimensions are in inches.)

EXPERIMENTAL BACKGROUND

General Description

The questions investigated in this report arose from an as-yet unpublished regeneratively-cooled rocket-heat-transfer project conducted at Lewis. In the thrust chambers employed, the fuel was first used to cool the walls before entering the combustion chamber. The coolant channels were designed nearly rectangular in cross section. The chamber as fabricated had grooves of considerable depth between the coolant channels. The general configuration of the thrust chamber, and the cross section of the coolant channel with grooves between channels, is shown in figures 1(a) and (b), respectively. Peripherally varying heat-transfer coefficients would be likely to occur with this geometry.

Also shown in figure 1(b) are the thermocouples used to obtain wall and coolant temperatures. In each chamber, these sensor groups were located at several axial locations in two of the coolant channels. In four firings at a chamber pressure of 60 pounds per square inch absolute and 12 percent fuel (the conditions summarized in table I) with the first experimental thrust chamber, the midspan wall thermocouple readings at the study section ranged from 1282° to 1630° R. Correspondingly, the quarter-span thermocouple readings were 1158° to 1568° R. Investigation of 22 pairs of readings at or near the study section in several thrust chambers and under several operating conditions showed that the quarter-span thermocouple read an arithmetical average value of approximately 120° less than the midspan thermocouple. Although the two temperatures were quite sensitive to operating conditions, the difference between them was remarkably constant. The wall temperatures are a function of the heat-transfer-coefficient distributions; the

TABLE I. - REFERENCED THRUST-CHAMBER OPERATING CONDITIONS FOR PROPELLANT MIXTURE OF 12 PERCENT HYDROGEN WITH LIQUID FLUORINE

Measured parameters	Values
Fluorine weight flow rate, lb/sec	2.55
Hydrogen weight flow rate, lb/sec	0.348
Combustion pressure, psia	60
Coolant static temperature at study section, $^{\circ}$R	330
Ambient air temperature, $^{\circ}$R	530
Computed parameters	
Combustion gas total temperature, $^{\circ}$R	6194
Combustion gas static temperature at study section, $^{\circ}$R	6090

TABLE II. - THERMOCOUPLE READINGS AT STUDY SECTION FOR SEVERAL THRUST CHAMBERS AND RUNS

[Nominal chamber pressure, 60 psia; arithmetical average of temperature differences, 122° R; median value of temperature differences, 133° R.]

Thrust chamber	Run	Fuel, percent	Midspan wall temperature, °R	Quarter-span wall temperature, °R	Temperature difference, °R
1	1	12	1599	1435	164
	2	12	1399	1263	136
	3	12	1630	1568	62
	4	12	1282	1158	124
	5	15	1188	1073	115
	6	15	1135	1005	130
	7	15	1286	1183	103
	8	15	1253	1144	109
2	9	18	[a]985	[a]805	180
	9	↓	[a]1058	[a]899	159
	9		[b]1137	[b]1056	81
	10		[a]1099	[a]941	158
	10		[b]1285	[b]1167	118
	10		[b]1106	[b]962	144
3	11	18	1100	931	169
	11	18	827	917	-90
4	12	12	1730	1587	143
	13	12	1272	1215	57
	14	15	1273	1108	165
	15	15	1253	1048	205
	15	15	1447	1281	166
	16	15	1175	1089	86

[a]Measurements taken 0.5 in. upstream of study section.
[b]Measurements taken 0.5 in. downstream of study section.

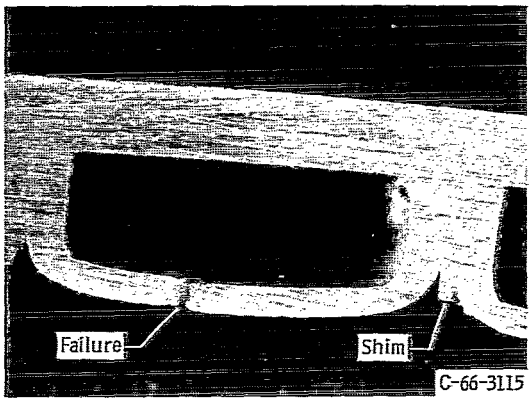

Figure 2. – Photograph of cross section of coolant channels showing typical failure near channel centerline.

average levels of the heat-transfer coefficients and temperatures depended on the operating conditions, but presumably the form of the coefficient and temperature distributions was more dependent on the chamber geometry. The thermocouple readings are listed in table II.

A channel section in the convergent region of the thrust chamber, near the throat, was chosen for this study. Experimentally, maximum heat-flux values occurred in the neighborhood of the study section; therefore, the effects of varying any parameter would be most obvious there. The particular thrust-chamber operating conditions used for this study were chosen because they yielded high heat-flux values and because data from several runs were available.

Channel failure patterns tended to confirm the temperature trends shown by the thermocouples. These failures took the form of axial cracks in the coolant channel bottoms, near the center of the channel, indicating that the highest wall temperatures and/or temperature gradients probably occurred there. A typical failure is shown in figure 2. These cracks occurred during firings at higher chamber pressures (300 psia) in which the wall temperatures were several hundred degrees higher. Insufficient data from these firings precluded performing this study under the more severe conditions.

Instrument Accuracy

A firm assessment of the accuracy of the installed thermocouples is not available. However, the possible sources of error may be discussed in qualitative terms. These sources include thermocouple size, the presence of excess braze, and the uncertainty of the thermocouple location.

As indicated previously, the thermocouple assemblies were placed in slots in the channel walls. The thermocouple outer diameter was 0.020 inch, while the wall thickness

was about 0.021 to 0.022 inch. The thermocouples were then brazed in place. The braze not only filled the remainder of the slots, but also tended to fill the interchannel grooves at the instrument locations. Thus, the installed sensors probably disturbed the system to some extent. However, the first condition was mitigated by two other factors. The thermocouple manufacturing method produced a mass of 304 stainless steel, of dimensions comparable to the thermocouple outside diameter, at the actual junction of the wire pairs (fig. 1(c)). Furthermore, the braze material used had a thermal conductivity approximately that of the channel wall. In the immediate vicinity of the junctions then, the different materials present had similar thermal conductivity values. An evaluation of the effects of the excess braze material is included in this report.

The third error source was the uncertainty of instrument location. There was some indication that some of the bent quarter-span thermocouple assemblies tended to straighten during brazing; this would move the junctions perhaps several thousandths of an inch closer to the gas side of the channel wall than was intended. It is therefore believed that location errors would tend to make the recorded quarter-span temperatures too high. There was no reason to believe that the midspan junction moved.

The point pertinent to this report is the observation that the mid-span wall temperature was higher than the quarter-span wall temperature. This result was obtained with many sets of thermocouples installed in several thrust chambers, as shown in table II (p. 5), and confirmed by channel failure patterns observed at higher chamber pressures.

METHOD OF ANALYSIS

Assumptions

The basic analytical problem was to determine the temperature distribution in the channel material when the fluid temperatures and heat-transfer-coefficient distributions around the boundaries were assumed. Because steady-state conditions were attained in the experimental thrust chambers, this analysis considered steady-state cases. Also, because the experimental axial-wall-temperature gradients were much smaller than the radial gradients, heat conduction along the chamber axis was neglected. It was further assumed that no quantity varied from channel to channel; consequently, because of symmetry, it was only necessary to study half a channel. Finally, in drawing a cross section for study, a flat channel bottom was assumed, as shown in figure 1(b) (p. 3). The slight curvature present in the channel bottom of figure 2 was neglected, and so was the possibility that internal pressure and thermal stress would cause additional bowing under operating conditions.

For most cases considered, thermal conductivity values for 304L stainless steel

(ref. 4) were used in the bottom and radial sides of the coolant channel, and those for 347 stainless steel (ref. 5) for the top, or outer cover, which in the actual chamber had been a wire wrapping of similar material (AM 350). The temperature dependence of thermal conductivity was accounted for in the calculations. The presence of braze material in the groove between channels was neglected in most cases. However, some calculations were repeated with the grooves completely filled to simulate excess braze present at the thermocouple installations. The braze was assumed to have the same conductivity as the channel wall. The two channel configurations are shown in figure 3.

For all cases, the heat-transfer coefficient used outside the wire wrap was calculated for a horizontal cylinder cooling in air. The choice of coolant and gas-side heat-transfer-coefficient distributions is discussed in the section CALCULATION PROCEDURE.

Equations and Solution Technique

The first law of thermodynamics combined with Fourier's law of heat conduction, for the assumptions of variable conductivity, no internal heat generation, and steady-state conditions, yields the expression for homogeneous materials:

$$\frac{\partial}{\partial x}\left(k\frac{\partial T}{\partial x}\right) + \frac{\partial}{\partial y}\left(k\frac{\partial T}{\partial y}\right) = 0 \tag{1}$$

(All symbols are defined in appendix A.) Although closed-form solutions to this equation have been obtained for simple cases of geometry, boundary conditions, and conductivity variations, a numerical solution appears the most attractive for the conditions assumed here. As indicated in figure 3, the section is covered by a network of lines, and the temperature at each intersection (point 0) is found in terms of the temperatures of the surrounding points (1, 2, 3, and 4). Equation (1) is by this means approximated as

$$(UA)_{1,0}\left(T_1 - T_0\right) + (UA)_{2,0}\left(T_2 - T_0\right) + (UA)_{3,0}\left(T_3 - T_0\right) + (UA)_{4,0}\left(T_4 - T_0\right) = 0 \tag{2a}$$

or

$$\sum (UA)_{i,0}\left(T_i - T_0\right) = 0 \tag{2b}$$

Here, U is an overall heat-transfer conductance and is a function of geometry, conductivity, and convective coefficients and is discussed in detail in appendix B.

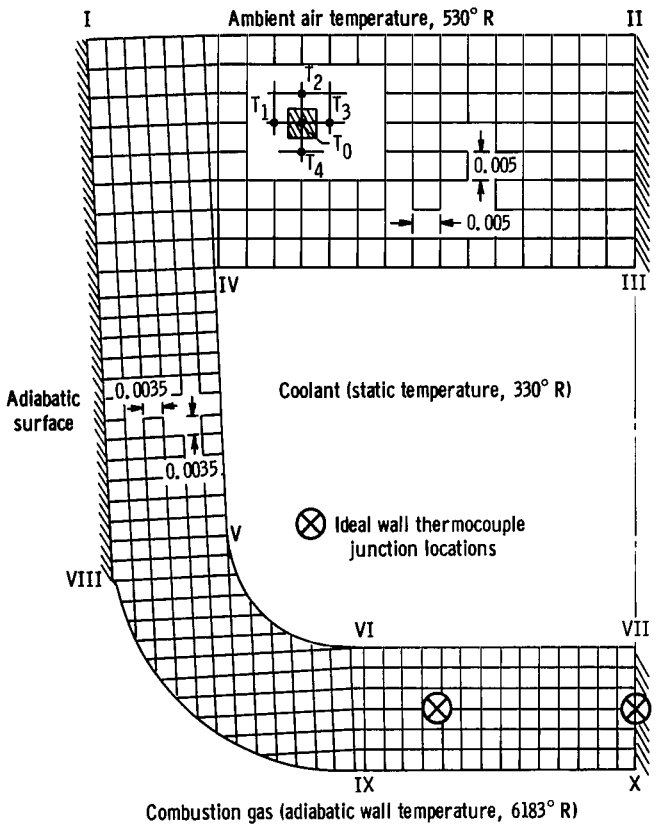

(a) Configuration with thermocouple braze material neglected.

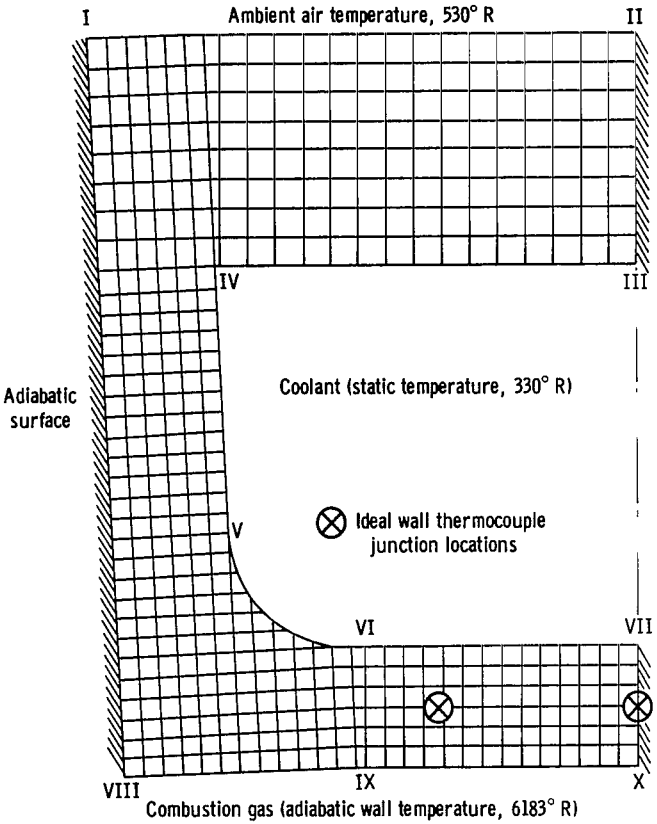

(b) Configuration with groove filled by thermocouple braze material.

Figure 3. - Coolant-channel cross section configurations assumed.

In iteratively solving the system of about 450 linear equations of the form of equation (2b), initially assumed temperatures or those obtained from a previous iteration are utilized. In general, the equation is almost never immediately satisfied, but an interim value of T_0, called here T_0', can be defined

$$T_0' = \frac{\sum (UA)_{i,0}\, T_i}{\sum (UA)_{i,0}}$$

which does satisfy it. Then, on the next pass through the equation system, a new value of T_0 is used for computing. This new quantity is

$$T_0(\text{New}) = T_0(\text{Original}) + \omega\left[T_0' - T_0(\text{Original})\right]$$

The constants $(UA)_{i,0}$ are not changed until a pass through the entire system has been completed to ensure reciprocity of the conductance values from one point to another.

If the quantity ω is 1, this method becomes the classical Gauss-Seidel iteration process described in reference 6. If ω is between 1 and 2, the method may be called "successive overrelaxation." This method is discussed in reference 7 and is there shown, in the linear case, to converge much more quickly than the Gauss-Seidel process for some optimum range of ω. For values greater than 2, however, the process diverges. A value of 1.4 was used in the calculations for this study. No attempt was made to find an optimum value, nor was a value of 1 tried to test the advantage of the method.

Accuracy of Solution

As mentioned earlier, the conductance factors were left unchanged until completion of a pass through the system of equations. Since the temperatures were changed point by point, in general the temperature and conductance values were not in strict correspondence. However, the thermal conductivity was not a rapidly changing function of temperature; therefore, this effect would become quite small as convergence proceeded. To minimize this error at the outset and to reduce the number of iterations required for convergence, care was taken to begin with reasonable temperature estimates.

In most cases, 2100 passes through the system of equations were performed. At this number of iterations, comparison of consecutive pass results revealed the average absolute value of the temperature corrections to be of the order of 0.0001° R. In the worst case, with all temperatures but one correct, the one error would then be of the

order of 0.05° R. A summation of heat input over the convective boundaries was also performed to provide another check. The heat flows into and out of the section agreed within about 2 percent.

This 2 percent error in heat flux persisted through several hundred additional iterations in a trial case and was felt to arise from the effect of grid size on the accuracy of the equations used. It is shown in reference 6 that, for expressions such as equations (2), the error in approximating the derivatives approaches zero as fast as the grid size for unequal spacing of the grid points, or as fast as the square of the grid size for equal spacing. Thus the error could be reduced by using a finer mesh.

CALCULATION PROCEDURE

Several parameters were varied individually to determine and compare their effects on coolant-channel wall-temperature and heat-flux distributions. First, three peripheral distributions of the coolant-side heat-transfer coefficient were investigated while the gas-side heat-transfer coefficient was held constant. Next, three gas-side-coefficient distributions were assumed, with the coolant-side coefficient held constant. The geometry shown in figure 3(a) was employed. Then the effects of the gas-side-coefficient distributions were reexamined by using the geometry of figure 3(b) to simulate the additional braze material present at thermocouple stations in the experimental thrust chambers. Finally, the former geometry and constant coolant and gas-side coefficients were used to explore the effects of changing the thickness and thermal conductivity of the channel wall. The first of 10 cases, with constant coefficients, the geometry of figure 3(a), and wall conductivity values of 304 stainless steel, was used as a control case with which to compare others. The heat-transfer coefficients used for the ambient air outside the thrust chamber were the same for all cases, as shown in figure 4(a).

Coolant-Side Heat-Transfer-Coefficient Variations

The first question considered was what effect a nonuniform coolant heat-transfer coefficient might have on the channel wall temperatures and on the heat rejection from the gas to the coolant. To answer this question, three peripheral distributions of the coefficient were assumed.

Constant coefficient. - In the first case, a constant heat-transfer coefficient was used. Its value was calculated from an expression for fully developed turbulent flow in tubes,

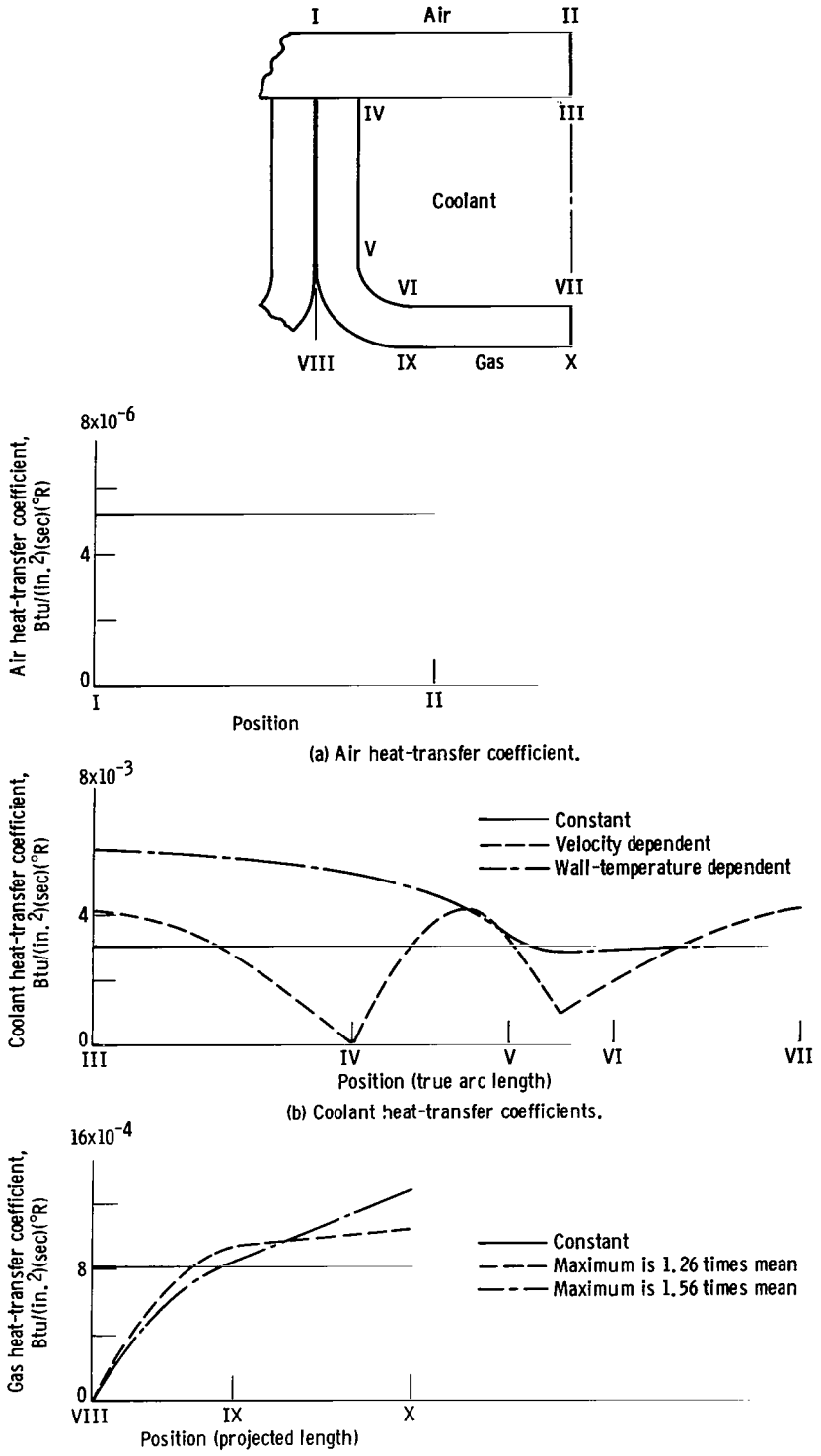

Figure 4. - Heat-transfer coefficient distributions assumed.

$$\left(\frac{hd}{k}\right)_f = 0.0267\left(\frac{Gd}{\mu_f}\frac{\rho f}{\rho_s}\right)^{0.8}\left(\frac{c_p\mu}{k}\right)_f^{0.333} \tag{3}$$

with properties evaluated at the film temperature

$$T_f = \frac{\left(T_s + T_{w,c}\right)}{2}$$

The wall temperature used was the calculated wall temperature at point VII in figure 3. The constant in equation (3) was determined, at the axial location in question, from the unpublished data previously mentioned. The coolant (hydrogen) properties were calculated by a computer program originally written for reference 8. The resulting constant heat-transfer coefficient is shown by the solid line in figure 4(b).

Coefficient dependent on velocity distribution. - When a fluid moves through a non-circular channel, the lines of constant velocity assume shapes depending on the channel geometry, and the velocity gradient at the wall is no longer constant over the entire periphery. In such circumstances, the heat flux may also be expected to vary over the periphery. (The heat flux may itself affect the velocity distribution, but such coupling will not be considered here.) In reference 2, the cases of square and triangular channels were analyzed. In both cases, the heat flux to the coolant varied from zero at the corners to a maximum at the midpoints of the walls, thus giving a large peripheral variation. To determine the effect of such a variation on wall temperature, the present analysis used a heat-transfer coefficient profile similar to the square-channel heat-flux distribution given in the reference. In addition, the heat-transfer coefficient profile assumed retained nonzero values in the bend region of the channel, since there is no actual corner there. Thus, some liberties were taken in applying the results of reference 2. The resulting average heat-transfer coefficient for the entire periphery was very nearly equal to the constant value assumed in the previous case. The profile is shown by the dashed line in figure 4(b).

Coefficient dependent on wall temperature. - In the third case, the large variation of wall temperature from top to bottom of the coolant channel was considered. Such a variation causes appreciable difference in the properties of the fluid in the layer next to the wall. For this reason, at each point on the surface, the film temperature was calculated by using the computed local wall temperature, and the heat-transfer coefficient was obtained at each point from the expression given earlier (eq. (3)). The resulting final distribution is shown in figure 4(b). This problem was the most complex to calculate of the

three coolant heat-transfer coefficient cases considered because both the surface temperatures and coefficients were initially unknown.

Gas-Side Heat-Transfer-Coefficient Variations

As noted earlier, it has been experimentally observed that the midspan wall thermocouple usually reported temperatures about 120° higher than those of the quarter-span thermocouple. The goal of the gas-side study was to find a heat-transfer-coefficient distribution that would yield approximately the experimental wall-temperature pattern.

The first distribution assumed was the constant coefficient used in the previously described coolant-side studies. Therefore, the first gas-side case was actually the control case. The value of the heat-transfer coefficient was determined from the expression

$$\left(\frac{hD}{k}\right)_r = 0.0307\left(\frac{GD}{\mu_r}\right)^{0.8}\left(\frac{T_s}{T_r}\right)^{0.8}\left(\frac{c_p\mu}{k}\right)_r^{0.333} \tag{4}$$

where

$$T_r = 0.5\left(T_s + T_w\right) + 0.22\sqrt[3]{\left(\frac{c_p\mu}{k}\right)_r}\left(T_t - T_s\right)$$

The constant in equation (4) was determined for the study section from the unpublished data previously mentioned and the reference temperature T_r is from a correlation method discussed in reference 9. The combustion-gas (hydrogen-fluorine) state at the study section was calculated by the methods of references 10 and 11, and properties were obtained by the method of reference 12. Equilibrium chemical composition was assumed.

Two varying distributions of the gas-side coefficient were also assumed. Each consisted of a sine function in the groove, or bend region of the channel, and a linear function in the flat bottom region. The sine-wave amplitudes and line slopes were so chosen that each distribution yielded an average value over the projected periphery, which was equal to the constant coefficient discussed in the preceding paragraph. The constant and two varying functions are shown in figure 4(c).

The varying functions were chosen because of the noncircular cross section of the thrust chamber. First, it is probable that the gas-side boundary layer would be thicker in the interchannel grooves than elsewhere. Second, if a layer of gas remained in a groove for any significant distance, it would become greatly cooled relative to the main

stream. Either effect would be equivalent to a reduction of the gas-side heat-transfer coefficient in the groove region.

The functions chosen admittedly have two deficiencies. First, the slopes of the linear functions could not be determined from inspection of the section geometry (fig. 3(a), p. 9). Second, at the side of the channel, neither a zero heat-transfer coefficient nor a cusp in the function seems physically likely to occur. For these reasons, it is not claimed that the functions accurately represent what actually occurs in the operating thust chamber. Yet, by comparing the resulting calculated temperature distributions with the experimental wall temperatures, it is possible to deduce that the heat-transfer coefficient varies appreciably between the center and the side of the channel.

After using the gas-side functions with the geometry of figure 3(a), two gas-side cases were then repeated by using the geometry shown in figure 3(b). This was done to represent the case in which the thermocouple braze filled the groove between channels, to determine whether the different geometry would account for the experimental temperature patterns.

Wall-Thickness and Thermal-Conductivity Effects

The thickness and thermal conductivity of the channel wall were varied in separate runs. In each case, the coolant and gas-side heat-transfer coefficients were constant over their respective surfaces. One case was run by using twice the thermal conductivity of 304 stainless steel, which approximated the conductivity of nickel. There was little reason to lower the conductivity because 304 stainless steel has approximately the same, relatively low, conductivity as many high-strength high-temperature alloys. One case was also performed by using half the wall thickness of the control case, with the channel internal dimensions held constant. Again, because a thin wall is desirable in a regeneratively cooled thrust chamber, there was no reason to investigate a thick-wall case.

RESULTS AND DISCUSSION

Coolant-Side Heat-Transfer Coefficients

Although the three assumed coolant-side heat-transfer-coefficient profiles were quite different, they yielded remarkably similar results, as shown by the temperature and heat-flux plots in figure 5. All three produced maximum coolant- and gas-side wall temperatures in the bend region of the channel, rather than at the middle of the bottom surface. The maximum gas-side wall temperatures varied by only 20^{o}. None of the cal-

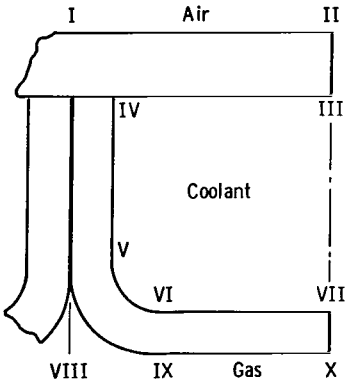

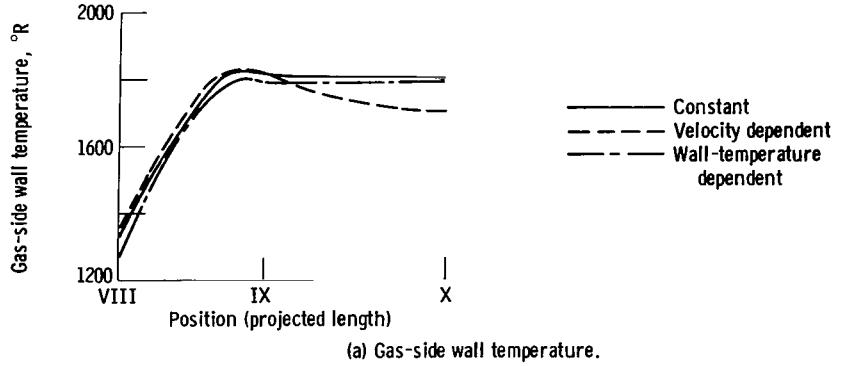

(a) Gas-side wall temperature.

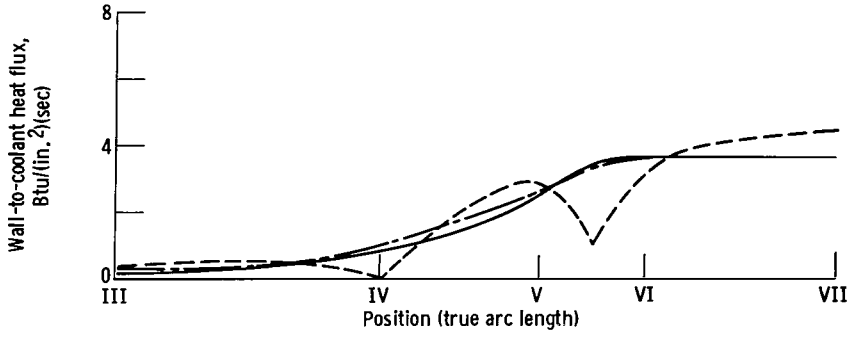

(b) Wall-to-coolant heat flux.

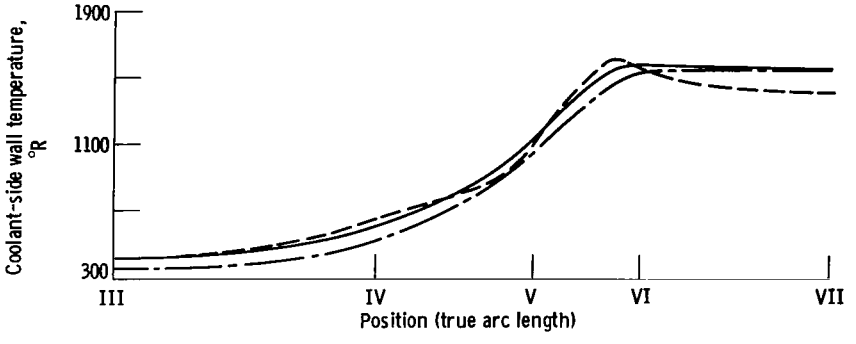

(c) Coolant-side wall temperature.

Figure 5. - Wall-temperature and heat-flux distributions obtained with assumed coolant heat-transfer coefficients.

culated temperature profiles agreed with the experimentally observed patterns. The constant and temperature-dependent coefficients gave nearly identical temperature and heat-flux profiles throughout most of the channel. The velocity-dependent heat-transfer coefficient gave somewhat different temperatures in the bottom region of the channel, producing low temperatures at the centerline because the coefficient was at a maximum there. For the velocity-dependent case, the variations in wall-to-coolant heat flux also differed from the other two and reflected the variation of the coefficient. The total heat transferred to the coolant was essentially the same for all three cases; the differences were no larger than the residual error in the calculations.

The equality of the total heat transfer for the three cases was a result of the difference between the gas and wall temperatures. This difference was so great that the heat input to the channel was very insensitive to the wall-temperature differences produced by the different coolant coefficients. The heat input from the ambient air outside the wire wrap was too small to affect this result.

The fact that the wall temperatures reached maximum values in the bend region is attributed to the geometry and to the low thermal conductivity of the wall. As may be noted in figure 1(b) (p. 3), the bend inner radius was equal to the wall thickness. In this region of the channel, then, the gas-side surface area was twice the coolant-side surface area. Because of this area difference, the heat input from the gas was not readily removed by the coolant, and a hot spot resulted. As shown later, the hot spot could be alleviated by either a thinner wall or a higher wall thermal conductivity.

In summary, the effects of a peripherally varying coolant heat-transfer-coefficient distribution were small because of the large gas-to-wall temperature difference and the channel geometry. Although the exact distribution that occurs is unknown, it appears entirely adequate here to assume that the coolant coefficient is constant over the periphery.

Gas-Side Heat-Transfer Coefficients

In contrast to the coolant cases, the gas-side heat-transfer-coefficient distributions assumed produced significant differences in the channel-wall-temperature patterns. For example, in figure 6, the case with constant gas-side coefficient (the control case), yielded a minimum gas-side wall temperature of 1350° R in the bottom of the interchannel groove, a maximum value of 1820° R in the bend region, and a slightly lower value of 1800° R at the channel centerline. The varying coefficients, with maximum to mean ratios of 1.26 and 1.56, gave maximum temperatures at the centerline, with values of 1890° and 1960° R, respectively. The wall-to-coolant heat-flux profiles changed some-

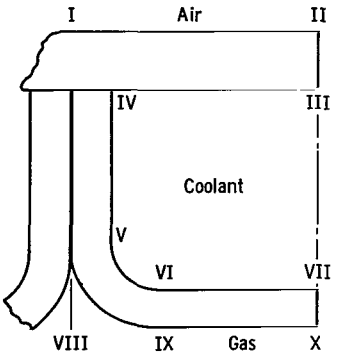

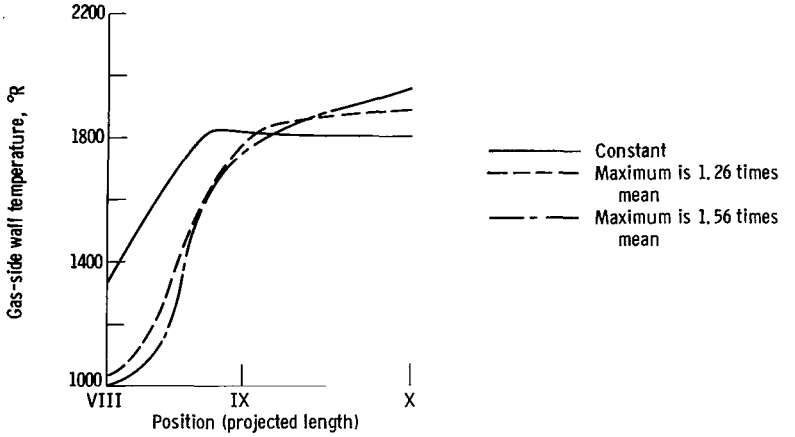

(a) Gas-side wall temperature.

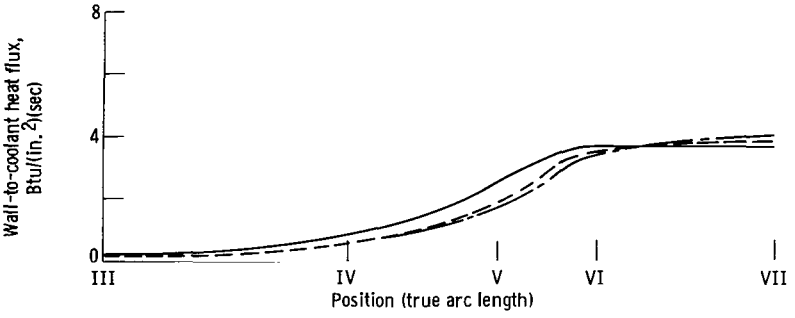

(b) Wall-to-coolant heat flux.

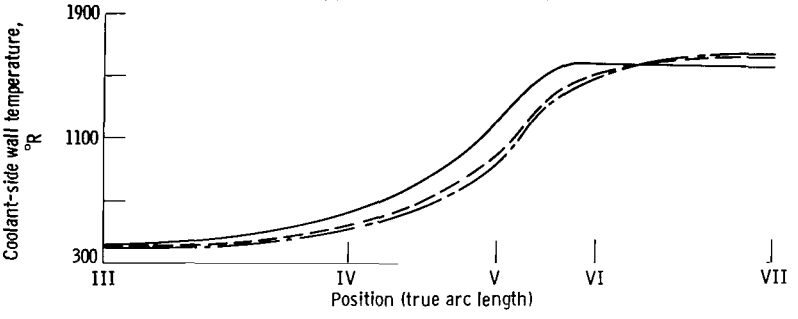

(c) Coolant-side wall temperature.

Figure 6. - Wall-temperature and heat-flux distributions obtained with assumed gas-side heat-transfer coefficients.

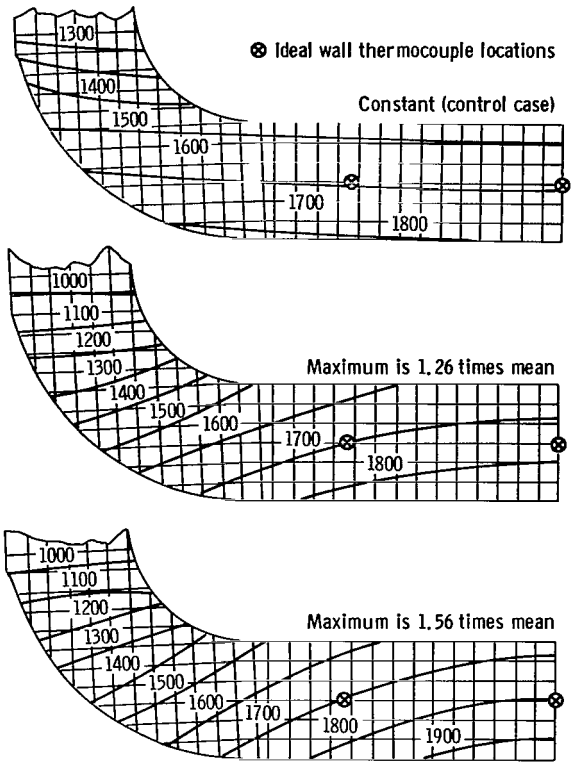

Figure 7. - Coolant-channel wall temperatures obtained with assumed gas-side heat-transfer coefficients.

what to reflect the varying gas-side-coefficient profiles, but not as greatly as the gas-side wall-temperature profiles. The total heat transfer to the coolant was approximately the same for all three cases.

The temperature trends, and the intended thermocouple junction locations, are shown in another form in figure 7. Of the three gas-side distributions assumed, the most rapidly changing function produced wall-temperature trends most like the experimental temperature patterns. The calculated difference between midspan and quarter-span wall temperatures was about 107° R, compared with the experimental average of 122° R. For comparison, the control case yielded a difference of -4° R (negative because the quarter-span wall temperature was higher than the midspan value).

The calculations with the constant and 1.56 gas-side heat-transfer-coefficient profiles were repeated by using the geometry shown in figure 3(b) (p. 9) to determine whether the excess braze present at thermocouple stations would change the wall-temperature profiles and affect the conclusions already reached. Constant coolant coefficients were again used for these cases. As in the previous case, the wall-temperature variations grew with increasing nonuniformity of the gas-side heat-transfer coefficients. Also, the 1.56 function again yielded temperature trends in better agreement with experimental data. The 1.56 heat-transfer-coefficient profile gave a temperature difference between thermocouple locations of 125° R, compared with a difference of 27° R obtained with the constant coefficient. Thus, the presence of the thermocouple braze material does not affect the conclusions derived from the previous geometry. The results are shown in figure 8.

The two cases differed principally in that the flat-bottom geometry had about 15 percent less gas-side surface area than the previous channel configuration. Thus, although the patterns of heat flux per unit area were much alike, the total heat transfer to the coolant was about 15 percent less for the flat-bottom case. It is therefore important in thrust-chamber design to specify the total gas-side surface area at each cross section with precision, otherwise the rate of coolant enthalpy rise may be miscalculated by an appreciable margin.

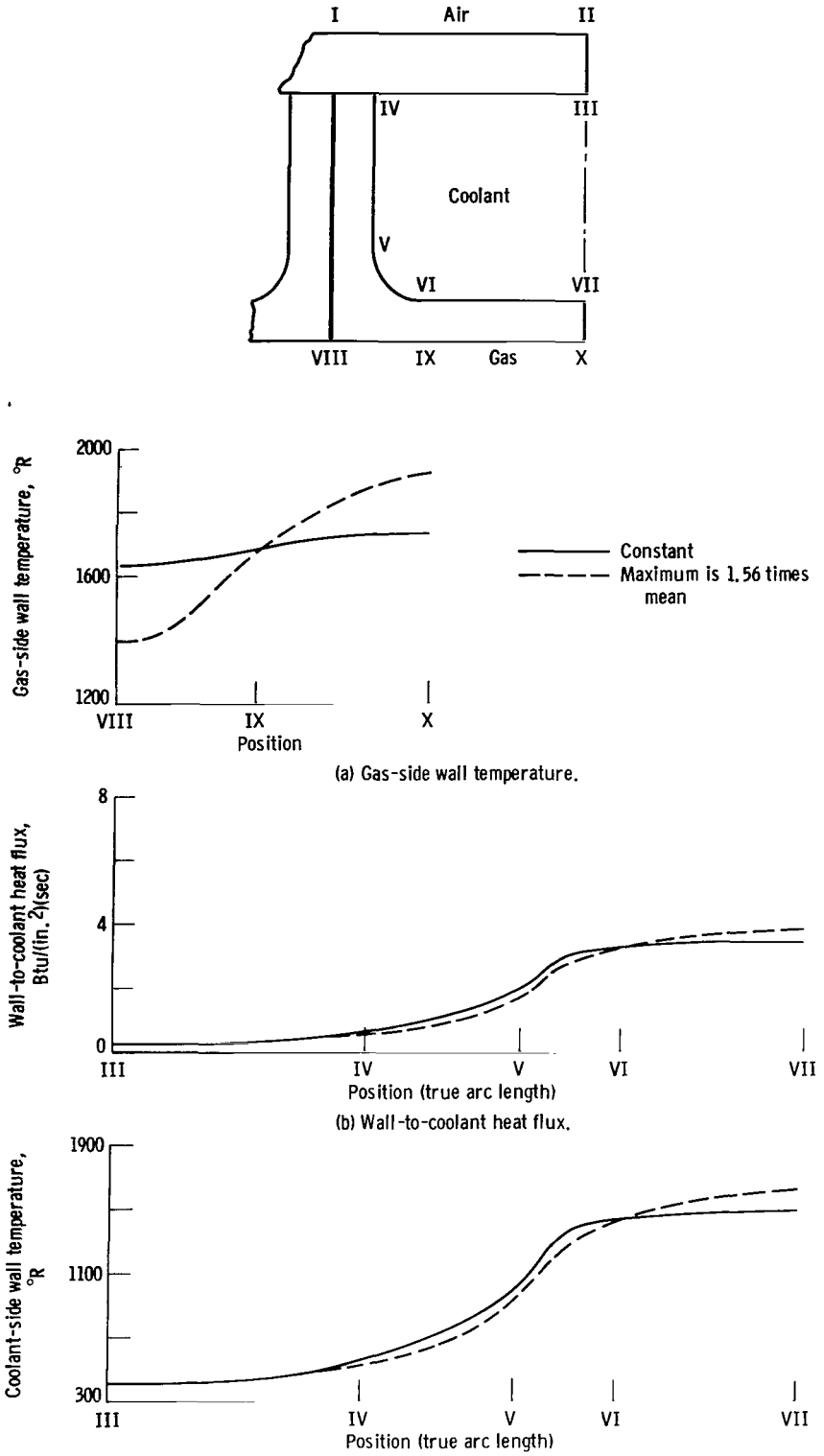

Figure 8. - Wall-temperature and heat-flux distributions obtained with flat-bottom channel cross section and assumed gas-side heat-transfer coefficients.

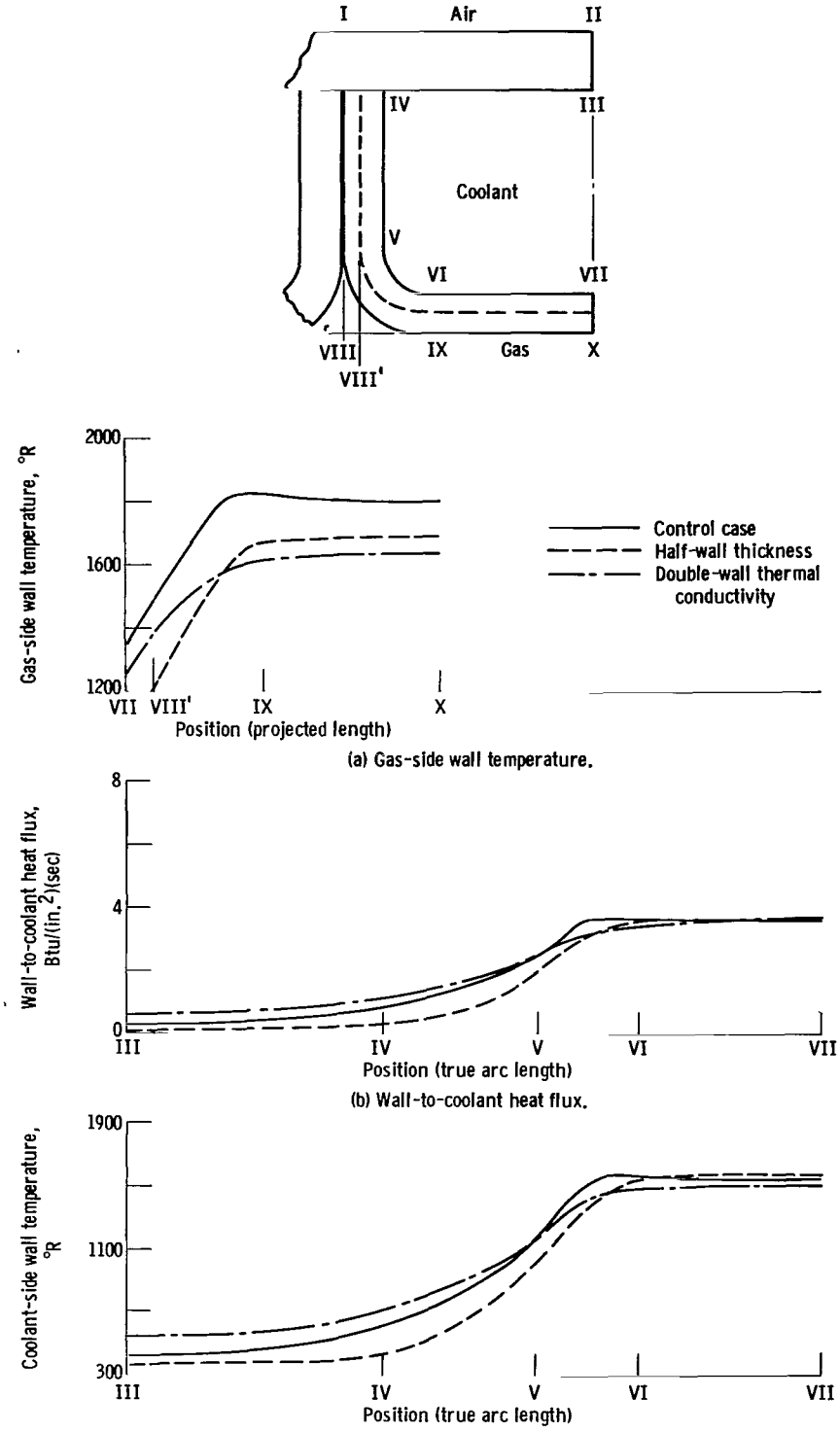

Figure 9. - Wall-temperature and heat-flux distributions obtained by changing coolant-channel wall thickness and thermal conductivity.

In summary, from a comparison of experimental temperature distributions with calculated results, it is concluded that a large variation of the gas-side heat-transfer coefficient may exist across the width of a coolant channel. For the cases considered here, failure to consider this variation resulted in underestimating the maximum gas-side wall temperature by about 140° R for the channel configuration with a groove, and by 190° R for the flat-bottom geometry. Of the heat-transfer-coefficient distributions assumed, the one giving the best agreement with experimental wall-temperature trends has a centerline-to-average ratio of 1. 56. Though the specific model used may not truly represent the actual heat-transfer-coefficient distribution, any other function chosen would require a similar centerline-to-average or centerline-to-side variation to produce experimental wall-temperature patterns. It is also concluded that the total heat transfer to the coolant can be miscalculated by a substantial margin if the gas-side surface area is not accurately specified.

Wall Thickness and Thermal Conductivity

The effects of doubling the wall thermal conductivity and the effects of halving the wall thickness were very similar, as expected. In both cases, the hot spot in the bend region was alleviated. The gas-side wall temperatures were reduced compared with the control case, while the coolant-side wall temperatures remained about the same. The wall-to-coolant heat flux was slightly greater than that for the control case, since the overall thermal conductance from gas to coolant was higher. The results are shown and compared with the control case in figure 9. As the sketch and part (a) in figure 9 indicate, the thinner-wall channel has less gas-side surface area. This accounts for the lower heat flux curve observed in figure 9(b). However, more such channels would be required to fabricate a chamber of the same gas-side dimensions.

SUMMARY OF RESULTS

Wall-temperature and heat-flux profiles in the cross section of a rocket-thrust-chamber coolant channel were determined by numerical methods. Several peripheral distributions of the coolant and gas-side heat-transfer coefficients were assumed, and the resulting wall-temperature patterns were compared with experimental measurements. The wall thickness and thermal conductivity of the channel material and the volume of the braze fillet were also varied. The conclusions are summarized as follows:

1. The gas-side heat-transfer coefficient was shown to vary appreciably over the width of the coolant channel.

2. Peripheral variations of the coolant heat-transfer coefficient were shown to have little effect on the maximum wall temperature.

3. To estimate the heat transferred to the coolant accurately, the gas-side surface area of the channel must be specified with precision.

Lewis Research Center,
National Aeronautics and Space Administration,
Cleveland, Ohio, July 27, 1966,
128-31-06-01-22.

APPENDIX A

SYMBOLS

A	area, sq in.
c_p	specific heat at constant pressure, Btu/(lb)(^{o}R)
D	thrust chamber internal diameter at section in question, in.
d	coolant channel hydraulic diameter at section in question; equal to four times flow cross section area, divided by wetted perimeter, in.
G	mass velocity of gas or coolant, lb/(in.^{2})(sec)
h	heat-transfer coefficient, Btu/(in.^{2})(sec)(^{o}R)
k	thermal conductivity, Btu/(in.)(sec)(^{o}R)
L	length of normal line from mesh point to convection surface, in.
ℓ	distance between two mesh points, in.
Q	heat flow, Btu/(sec)
T	temperature, ^{o}R
U	overall heat-transfer conductance, Btu/(in.^{2})(sec)(^{o}R)
ΔX	horizontal distance between grid points
x	horizontal coordinate
ΔY	vertical distance between grid points
y	vertical coordinate
μ	viscosity, lb/(in.)(sec)
ρ	density, lb/in.^{3}
ω	relaxation constant (dimensionless)
I, II, etc.	locations on cross sections

Subscripts:

c	coolant
F	fluid temperature
f	film temperature (for evaluation of properties)
g	gas (combustion gas)
i	neighboring point on grid
r	reference temperature (for evaluation of properties)
s	static
t	total
w	wall
0	central point on grid
1, 2, 3, 4	neighboring points on grid

Superscript:

'	interim value

APPENDIX B

GRID AND EQUATIONS USED IN COMPUTATION

Grid Construction

The gridwork used for the finite-difference equations in this study was constructed to exploit the several straight-line boundaries of the channel cross section and to aline the mesh with those surfaces. The mesh is illustrated in figure 3 (p. 9). In the curved region of the section, the use of circular coordinates would have been a natural choice; however, the rectangular coordinates were retained to reduce the amount of reprogramming that might have been necessary to accommodate a fillet of any shape on the combustion-gas side of the bend.

The grid construction employed here also permitted the channel section to be broken up into several rectangular or trapezoidal subsections; this simplified some of the programming instructions. However, a few irregular transition areas were left, and the grid points of adjacent subsections had to be overlapped to ensure continuity of temperature.

Sample Equations

Although the solution to the system of finite-difference equations was described in the text, the equations themselves were indicated in general terms. The important matter is the evaluation of the quantity UA, the coefficient of the temperature difference term for each point-to-point path in the problem. Three examples chosen from the cases encountered will illustrate the derivation of these.

The simplest case is a point within the wall material with a square mesh, as shown in figure 10(a). Fourier's expression for one-dimensional heat conduction between two points is

$$Q = k \frac{A}{\ell} \Delta T$$

In the case at hand, the path area (for unit depth normal to the drawing) is equal to the mesh length. The distance between points is also equal to the mesh length. Thus, the expression for net heat flow into the shaded element in the figure is

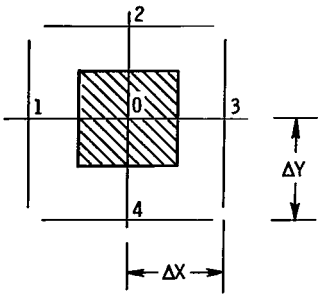

(a) Internal point.

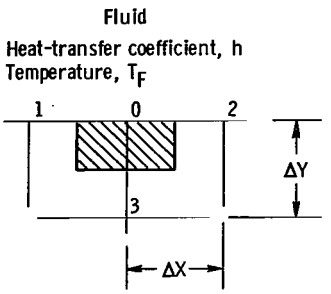

(b) Point on surface with convection.

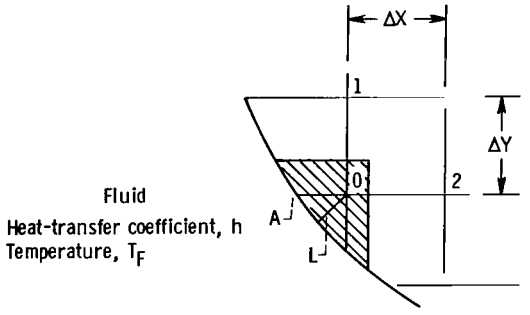

(c) Point near curved surface with convection.

Figure 10. - Typical grid situations encountered in finite-difference computations with configuration studied.

$$Q = k_{1,0}\left(T_1 - T_0\right) + k_{2,0}\left(T_2 - T_0\right) + k_{3,0}\left(T_3 - T_0\right) + k_{4,0}\left(T_4 - T_0\right)$$

where

$$k_{i,0} = \frac{k\left(T_i\right) + k\left(T_0\right)}{2}$$

is the value of conductivity between the points 0 and i. In this case, the conductance coefficients between points are the average conductivities. Also, in steady state the net heat flow is equal to zero.

Figure 10(b) shows a point on a convective surface, with a square or rectangular mesh. Here the net heat flow into the shaded area is given by

$$Q = h\Delta X\left(T_F - T_0\right) + k_{1,0}\frac{\Delta Y}{2\Delta X}\left(T_1 - T_0\right) + k_{2,0}\frac{\Delta Y}{2\Delta X}\left(T_2 - T_0\right) + k_{3,0}\frac{\Delta X}{\Delta Y}\left(T_3 - T_0\right)$$

Here, one of the conductance values is equal to the film coefficient times the mesh length. If, in addition, the line joining points 0 and 3 is an adiabatic surface (axis of symmetry), the equation remains the same but T_1 equals T_2 and $k_{1,0}$ equals $k_{2,0}$. Point 1 or 2 is then actually outside the boundary of the channel section, but is included as a fictitious point.

The third case in figure 10(c) occurs in the bend region of the section and is set up as follows. First, the heat flux from the fluid to the wall is given by

$$\frac{Q}{A} = h\left(T_F - T_w\right)$$

However, the point in question is not on the surface. If one-dimensional conduction to that point and equal areas for conduction and convection are assumed, with conductivity evaluated at temperature T_0 to avoid an extra iterative loop, the heat flux is

$$\frac{Q}{A} = \frac{k_0}{L}\left(T_w - T_0\right)$$

With some manipulation, the total heat flow into the shaded region may then be expressed as

$$Q = \frac{hA}{1 + \frac{hL}{k_0}}\left(T_F - T_0\right) + k_{1,0}\left(\frac{A}{\ell}\right)\left(T_1 - T_0\right) + k_{2,0}\left(\frac{A}{\ell}\right)_{2,0}\left(T_2 - T_0\right)$$

Here the area-length ratios, convection area, distance from the point to the surface, and heat-transfer coefficient are specific to each such point and must be supplied as data. This case is in contrast to the first case in which the geometrical quantities are all identical and need not be considered.

REFERENCES

1. Schacht, Ralph L.; Quentmeyer, Richard J.; and Jones, William L.: Experimental Investigation of Hot-Gas Side Heat-Transfer Rates for a Hydrogen-Oxygen Rocket. NASA TN D-2832, 1965.

2. Deissler, Robert G.; and Taylor, Maynard F.: Analysis of Turbulent Flow and Heat Transfer in Noncircular Passages. NACA TN 4384, 1958.

3. Eckert, E. R. G.; and Irvine, T. F., Jr.: Pressure Drop and Heat Transfer in a Duct with Triangular Cross Section. J. Heat Transfer, vol. 82, no. 2, May 1960, pp. 125-138.

4. Eckert, Ernst R. G.; and Drake, Robert M., Jr.: Heat and Mass Transfer. 2nd ed., McGraw-Hill Book Co., Inc., 1959.

5. Tebo, F. J.: Selected Values of the Physical Properties of Various Materials. Rep. No. ANL-5914, Argonne National Laboratory, Sept. 1958.

6. Salvadori, Mario G.; and Baron, Melvin L.: Numerical Methods in Engineering. Prentice-Hall, Inc., 1959.

7. Varga, Richard S.: Matrix Iterative Analysis. Prentice-Hall, Inc., 1962.

8. Curren, Arthur N.; Price, Harold G., Jr.; and Douglass, Howard W.: Analysis of Effects of Rocket-Engine Design Parameters on Regenerative-Cooling Capabilities of Several Propellants. NASA TN D-66, 1959.

9. Eckert, Ernst R. G.: Survey on Heat Transfer at High Speeds. (AF ARL-189), University of Minnesota, Dec. 1961.

10. Zeleznik, Frank J.; and Gordon, Sanford: A General IBM 704 or 7090 Computer Program for Computation of Chemical Equilibrium Compositions, Rocket Performance, and Chapman-Jouguet Detonations. NASA TN D-1454, 1962.

11. Gordon, Sanford; and Zeleznik, Frank J.: A General IBM 704 or 7090 Computer Program for Computation of Chemical Equilibrium Compositions, Rocket Performance, and Chapman-Jouguet Detonations. Supplement I - Assigned Area-Ratio Performance. NASA TN D-1737, 1963.

12. Svehla, Roger A.: Thermodynamic and Transport Properties for the Hydrogen-Oxygen System. NASA SP-3011, 1964.

NASA-Langley, 1966 E-3358

"The aeronautical and space activities of the United States shall be conducted so as to contribute . . . to the expansion of human knowledge of phenomena in the atmosphere and space. The Administration shall provide for the widest practicable and appropriate dissemination of information concerning its activities and the results thereof."

—NATIONAL AERONAUTICS AND SPACE ACT OF 1958

NASA SCIENTIFIC AND TECHNICAL PUBLICATIONS

TECHNICAL REPORTS: Scientific and technical information considered important, complete, and a lasting contribution to existing knowledge.

TECHNICAL NOTES: Information less broad in scope but nevertheless of importance as a contribution to existing knowledge.

TECHNICAL MEMORANDUMS: Information receiving limited distribution because of preliminary data, security classification, or other reasons.

CONTRACTOR REPORTS: Technical information generated in connection with a NASA contract or grant and released under NASA auspices.

TECHNICAL TRANSLATIONS: Information published in a foreign language considered to merit NASA distribution in English.

TECHNICAL REPRINTS: Information derived from NASA activities and initially published in the form of journal articles.

SPECIAL PUBLICATIONS: Information derived from or of value to NASA activities but not necessarily reporting the results of individual NASA-programmed scientific efforts. Publications include conference proceedings, monographs, data compilations, handbooks, sourcebooks, and special bibliographies.

Details on the availability of these publications may be obtained from:

SCIENTIFIC AND TECHNICAL INFORMATION DIVISION

NATIONAL AERONAUTICS AND SPACE ADMINISTRATION

Washington, D.C. 20546